Partial-wave analysis of pion photoproduction

Richard A. Arndt, Ron L. Workman, Zhujun Li, and L. David Roper
Department of Physics, Virginia Polytechnic Institute and State University, Blacksburg, Virginia 24061
(Received 30 March 1989)

An energy-dependent partial-wave analysis of pion photoproduction data through the second-resonance region (0–1 GeV laboratory kinetic energy) is presented. A set of energy-independent analyses has also been obtained starting from the energy-dependent solution. The data set contains 9074 data for the reactions $\gamma+p\to p+\pi^0$, $\gamma+p\to n+\pi^+$, $\gamma+n\to n+\pi^0$, $\gamma+n\to p+\pi^-$, and the inverse reaction $\pi^-+p\to n+\gamma$ (converted to $\gamma+n\to p+\pi^-$). The predictions of our solutions are compared with the results of previous analyses. Suggestions are made for future experiments.

I. INTRODUCTION

In this paper we describe an energy-dependent analysis of pion photoproduction data through the second resonance region (0–1 GeV laboratory kinetic energy). We also present the results of a set of energy-independent analyses carried out over the same energy range.

In the first resonance region, the dominant multipoles are now reasonably well determined for the photoproduction of pions from proton targets. However, neutron target data are still comparatively sparse; one must generally rely on isospin symmetry and the $I=\frac{3}{2}$ proton multipoles in order to obtain a good fit. Above a laboratory photon energy of about 450 MeV, the analyses are complicated by the breakdown of Watson's theorem. In this energy region there are contributions due to higher inelastic resonances as well as threshold behavior, such as the η-production cusp.

Numerous energy-dependent and energy-independent analyses have probed the first- and second-resonance regions and beyond. Fixed-t dispersion relations have often been used.[1,2] Perhaps the most sophisticated of these analyses has been carried out by Arai and Fujii.[3] Here a K-matrix formalism was used with a Regge parametrization of the high-energy amplitudes. Other authors have added a Breit-Wigner plus background contribution to the Born amplitude. Unfortunately, these methods satisfy Watson's theorem only approximately.

Energy-independent analyses tend to be less model dependent and may enforce Watson's theorem where valid, at each energy, in all partial waves. At a few energies there are sufficient data to fit[4] the photoproduction multipoles without resorting to Watson's theorem. Unfortunately, however, this is generally not possible. One usually bins the available data obtaining a grid of solutions. Berends and Donnachie[5] have extended this procedure into the second-resonance region by imposing Watson's theorem on the elastic partial waves, allowing a departure in only those multipoles influenced by inelasticity.

It is difficult to systematically compare the results of energy-dependent and energy-independent analyses for several reasons. Different authors have chosen different data bases for their analyses and have treated statistical and systematic errors in a variety of ways. In some cases data sets have been renormalized and pseudo-data have been added in order to make the energy-independent solutions more continuous. In many cases, the resulting multipoles have been quoted without errors.

By presenting both energy-dependent and energy-independent solutions we have reduced the model dependence. The energy-independent solutions also allow a check for missing structure in the energy-dependent solution. A summary of our solutions is given herein. More details are available from the authors.[6]

Our data base is described in the next section and a review of the pion photoproduction formalism is given in Sec. III. In Sec. IV we describe the parametrization used in our energy-dependent analysis. Our solutions are described in Sec. V. Here, also, fits to selected data are displayed. In Sec. VI we compare our solutions to previous analyses and make suggestions for future experiments. In Appendix A we give the relations required to convert between the various existing notations and conventions. Motivation for our energy-dependent parametrization is described in Appendix B.

II. PION PHOTOPRODUCTION DATA BASE

We have used the data compilation of Ukai and Nakamura[7] as the foundation of our data base.[6] However, some data have also been taken from the earlier compilation of Menze, Pfeil, and Wilcke.[8] Included are 9074 data for the reactions $\gamma+p\to p+\pi^0$, $\gamma+p\to n+\pi^+$, $\gamma+n\to n+\pi^0$, $\gamma+n\to p+\pi^-$ and the inverse reaction $\pi^-+p\to n+\gamma$ (converted to $\gamma+n\to p+\pi^-$). In addition to differential $[\sigma(\theta)=d\sigma/d\Omega]$ and total (σ_T) cross section data, we have included the available single (P, Σ, and T) and double (G and H) polarization measurements. Scatterplots of the available data are shown in Fig. 1 and a summary of the number and types of data analyzed in each of the reaction channels is given in Table I.

Not all of the available data were used in our analyses. Data taken before 1960 were removed, as were all single-angle and single-energy differential cross section measurements prior to 1970. Redundant data, such as any total

cross section data that were simply integrations of differential cross sections already included, were removed. Some individual data points were also deleted when their conflict with the rest of the data base could not be reconciled.

While we have considerably more asymmetry data than were analyzed by Arai and Fujii,[3] particular observables are still lightly populated. For the reaction $\gamma+n\to p+\pi^-$ very little P and T data exist in the first-resonance region and few P measurements exist away from 90° over the energy range of our analysis. The data gaps can most easily be seen in Fig. 1. Of course measurements at very forward and backward angles would be difficult as P, Σ, T, G, and H are all constrained to zero at 0° and 180°. Recent precise left-right asymmetry data[9] from the reaction $\pi^-p\to n\gamma$ has helped to choose between the various partial-wave analyses and model calculations. Its effect will be discussed in Sec. VI.

III. FORMALISM

In our analyses we determine the electric ($E_{l\pm}$) and magnetic ($M_{l\pm}$) multipole amplitudes (l=angular momentum of the final πN state and $j=l\pm\frac{1}{2}$). From them one can construct the helicity amplitudes:[10,11]

$$
\begin{aligned}
H_N(\theta)&=\sqrt{\tfrac{1}{2}}\cos\tfrac{1}{2}\theta\sum_{l=0}^{\infty}[(l+2)E_{l+}+lM_{l+}+lE_{(l+1)-}-(l+2)M_{(l+1)-}](P'_l-P'_{l+1})\ ,\\
H_{SP}(\theta)&=\sqrt{\tfrac{1}{2}}\cos\tfrac{1}{2}\theta\sin\theta\sum_{l=1}^{\infty}[E_{l+}-M_{l+}-E_{(l+1)-}-M_{(l+1)-}](P''_l-P''_{l+1})\ ,\\
H_{SA}(\theta)&=\sqrt{\tfrac{1}{2}}\sin\tfrac{1}{2}\theta\sum_{l=0}^{\infty}[(l+2)E_{l+}+lM_{l+}-E_{(l+1)-}+(l+2)M_{(l+1)-}](P'_l+P'_{l+1})\ ,\\
H_D(\theta)&=\sqrt{\tfrac{1}{2}}\sin\tfrac{1}{2}\theta\sin\theta\sum_{l=1}^{\infty}[E_{l+}-M_{l+}+E_{(l+1)-}+M_{(l+1)-}](P''_l+P''_{l+1})\ ,
\end{aligned}
\tag{3.1}
$$

where the subscript N means nonspin-flip; D, double-spin-flip; SP, spin-flip with photon and initial nucleon having parallel spins; and SA, spin-flip with photon and initial nucleon having antiparallel spins. These amplitudes are related to those of Walker[11] with the correspondence

$$H_1\equiv H_{SP},\quad H_2\equiv H_N,\quad H_3\equiv H_D,\quad H_4\equiv H_{SA}\ .$$

The four possible reaction channels can be described in terms of three isospin amplitudes:

$$
\begin{aligned}
&H^{\pi^0p}={}_pH^{1/2}+\tfrac{2}{3}H^{3/2},\quad H^{\pi^+n}=\sqrt{2}({}_pH^{1/2}-\tfrac{1}{3}H^{3/2})\ ,\\
&H^{\pi^-p}=\sqrt{2}({}_nH^{1/2}+\tfrac{1}{3}H^{3/2}),\quad H^{\pi^0n}=\tfrac{2}{3}H^{3/2}-{}_nH^{1/2}\ .
\end{aligned}
\tag{3.2}
$$

The superscripts $\frac{1}{2}$ and $\frac{3}{2}$ refer to the isospin and the subscripts n and p differentiate between the isospin $\frac{1}{2}$ amplitudes for neutron and proton targets.

The observables are then given in terms of the following bilinear combinations of the helicity amplitudes:[12]

$$
\begin{aligned}
\sigma(\theta)&=\frac{q}{2k}[|H_N(\theta)|^2+|H_D(\theta)|^2+|H_{SP}(\theta)|^2\\
&\qquad+|H_{SA}(\theta)|^2]\ ,\\
P(\theta)\sigma(\theta)&=-\frac{q}{k}\mathrm{Im}[H_{SP}(\theta)H_D^*(\theta)+H_N(\theta)H_{SA}^*(\theta)]\ ,\\
\Sigma(\theta)\sigma(\theta)&=\frac{q}{k}\mathrm{Re}[H_{SP}(\theta)H_{SA}^*(\theta)-H_N(\theta)H_D^*(\theta)]\ ,\\
T(\theta)\sigma(\theta)&=\frac{q}{k}\mathrm{Im}[H_{SP}(\theta)H_N^*(\theta)+H_D(\theta)H_{SA}^*(\theta)]\ ,\\
G(\theta)\sigma(\theta)&=-\frac{q}{k}\mathrm{Im}[H_{SP}(\theta)H_{SA}^*(\theta)+H_N(\theta)H_D^*(\theta)]\ ,\\
H(\theta)\sigma(\theta)&=-\frac{q}{k}\mathrm{Im}[H_{SP}(\theta)H_D^*(\theta)+H_{SA}(\theta)H_N^*(\theta)]\ .
\end{aligned}
\tag{3.3}
$$

TABLE I. Number of data used in our analyses (total=9074).

	$\sigma(\theta)$	$P(\theta)$	$\Sigma(\theta)$	$T(\theta)$	$G(\theta)$	$H(\theta)$	σ_T	Total
$\gamma p\to n\pi^+$	3374	161	406	373	32	89	7	4442
$\gamma p\to p\pi^0$	1712	404	279	197	0	0	39	2631
$\gamma n\to p\pi^-$	1533	59	152	83	0	0	54	1881
$\gamma n\to n\pi^0$	120	0	0	0	0	0	0	120

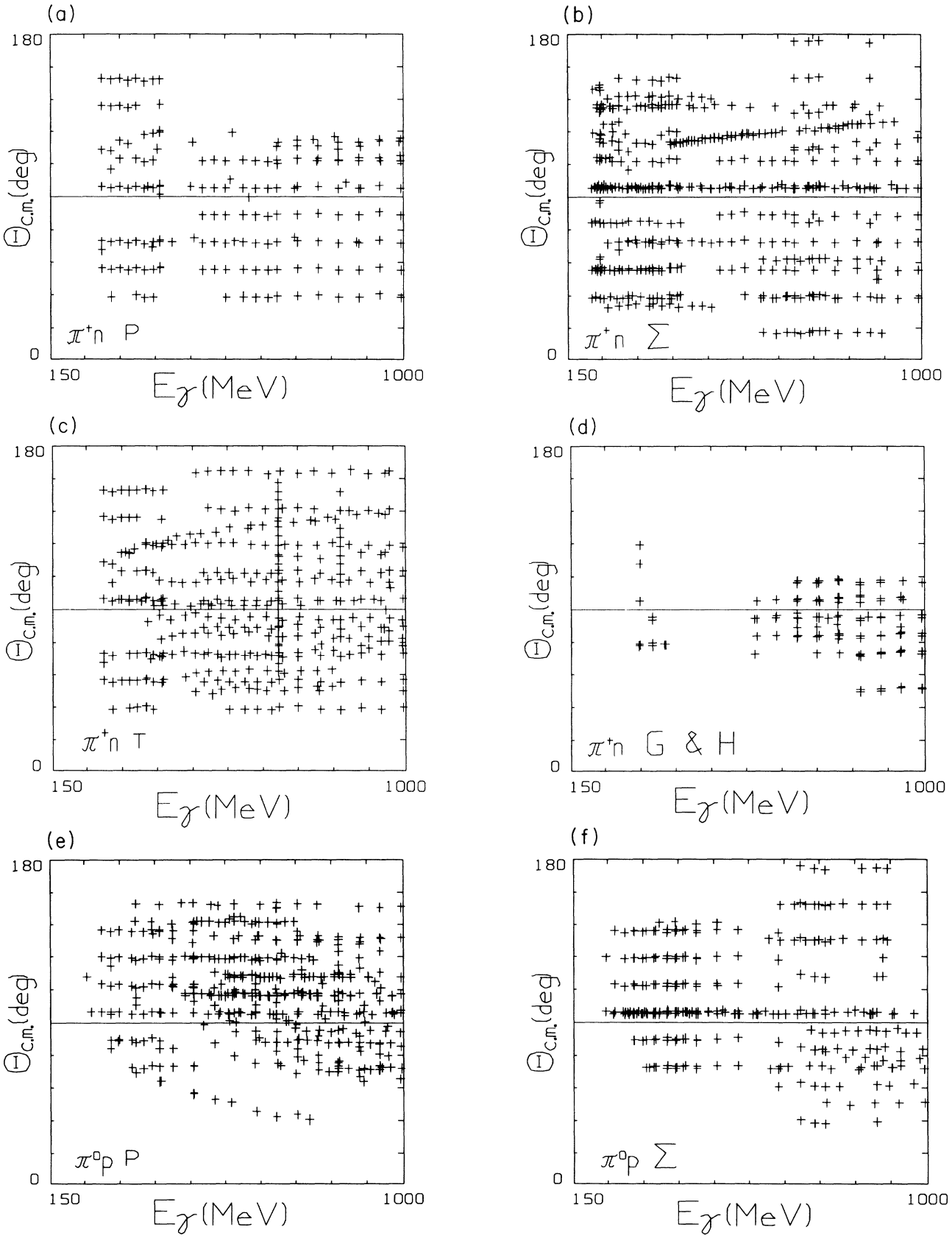

FIG. 1. Scatterplots (number of data versus photon energy and angle) for pion photoproduction. The scatterplots for $\gamma p \to \pi^+ n$, $\gamma p \to \pi^0 p$, and $\gamma n \to \pi^- p$ differential cross section are not shown because they are very dense. (a) $\gamma p \to \pi^+ n$, $P(\theta)$; (b) $\gamma p \to \pi^+ n$, $\Sigma(\theta)$; (c) $\gamma p \to \pi^+ n$, $T(\theta)$; (d) $\gamma p \to \pi^+ n$, $G(\theta)$ and $H(\theta)$; (e) $\gamma p \to \pi^0 p$, $P(\theta)$; (f) $\gamma p \to \pi^0 p$, $\Sigma(\theta)$; (g) $\gamma p \to \pi^0 p$, $T(\theta)$; (h) $\gamma n \to \pi^- p$, $P(\theta)$; (i) $\gamma n \to \pi^- p$, $T(\theta)$; (j) $\gamma n \to \pi^- p$, $\Sigma(\theta)$; (k) $\gamma n \to \pi^0 n$, $\sigma(\theta)$.

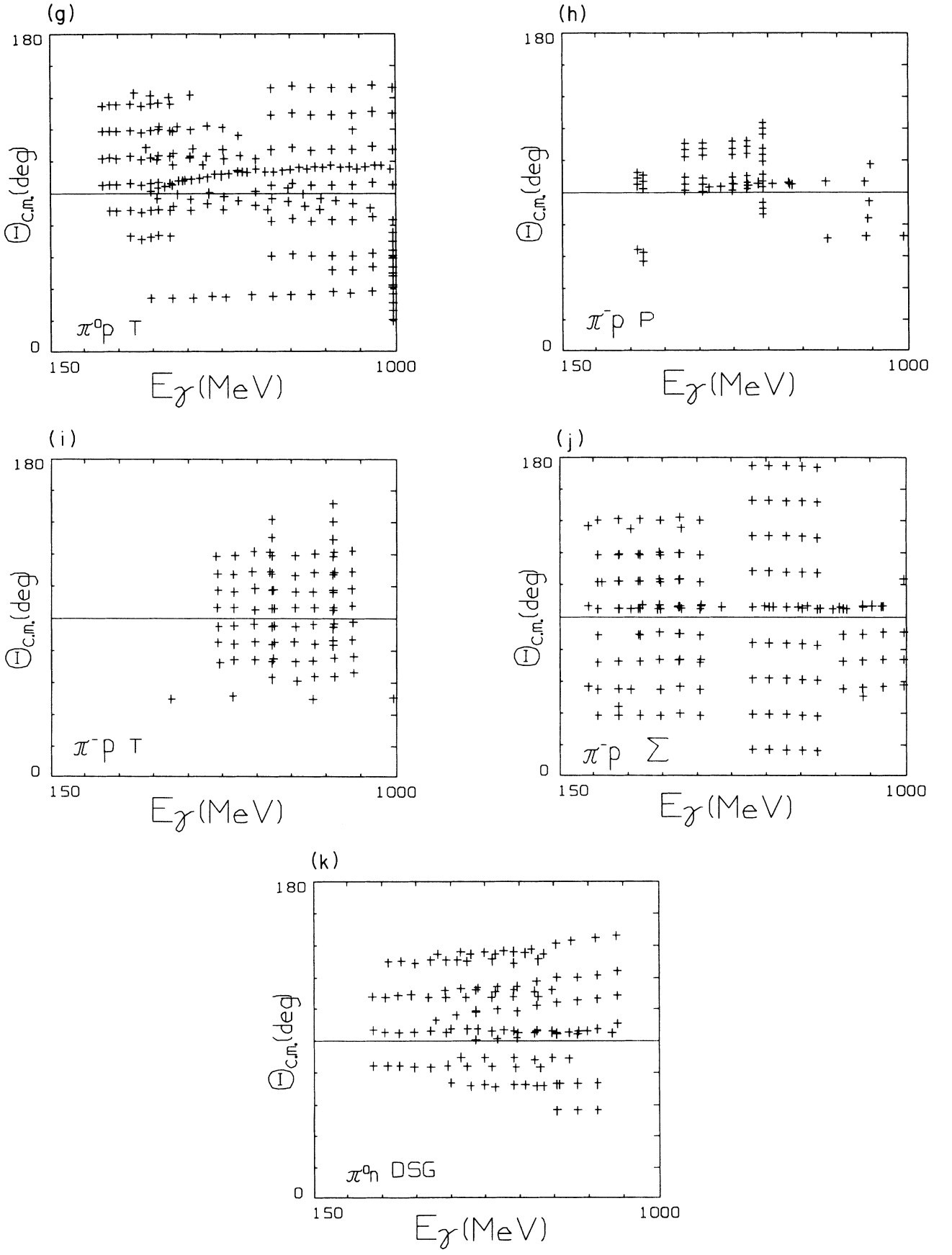

FIG. 1. (*Continued*).

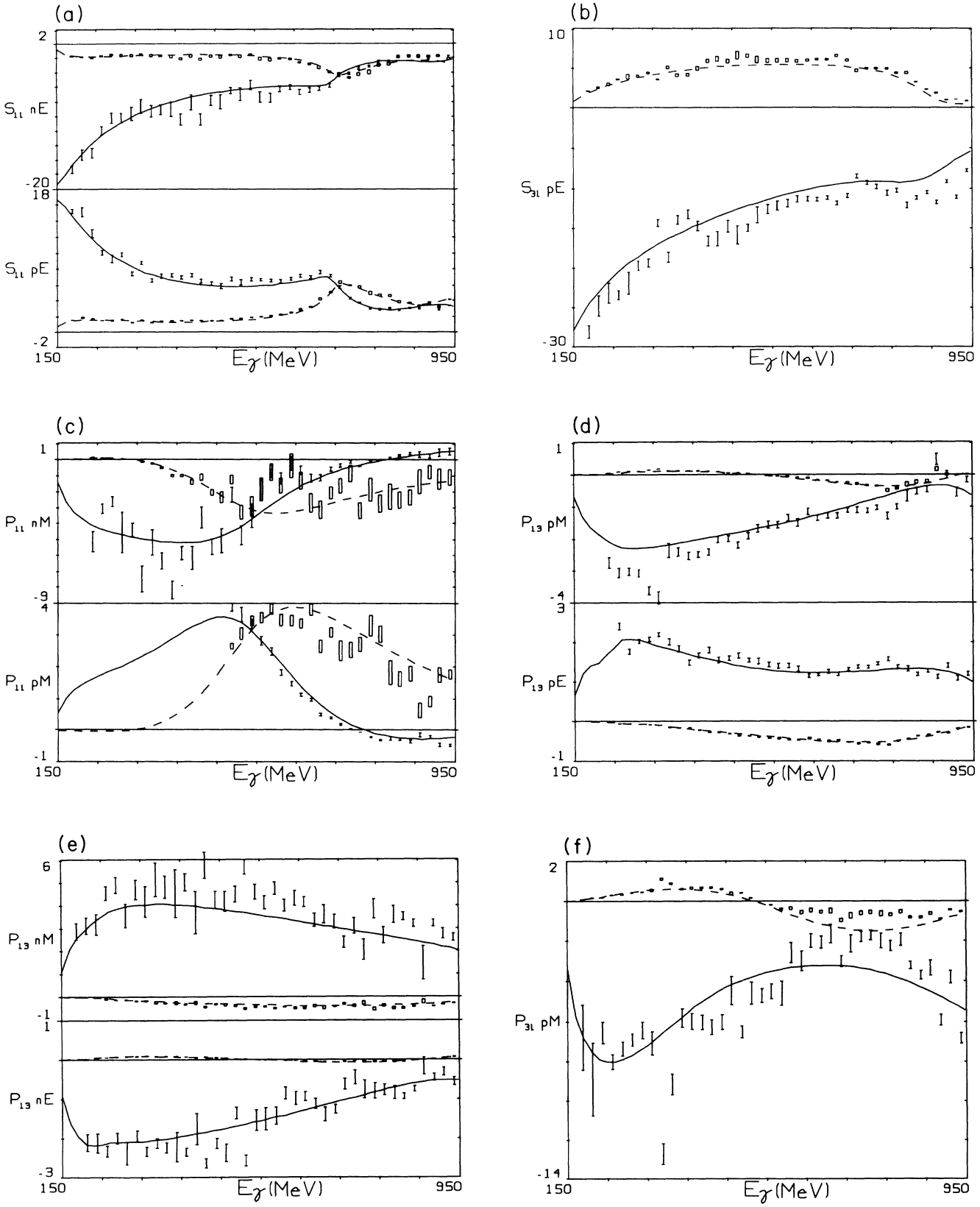

FIG. 2. Our multipole solutions in millifermi units. The notation is $L_{2I,2J}$ for πN followed by the multipole notation (target, multipole) for pion photoproduction. The real part of the amplitude is the solid curve and the imaginary part is the dashed curve. The error bars and boxes indicate our energy-independent solutions. (a) S_{11} (pE and nE), (b) $S_{31}pE$, (c) P_{11} (pM and nM), (d) P_{13} (pE and pM), (e) P_{13} (nE and nM), (f) $P_{31}pM$, (g) P_{33} (pE and pM), (h) D_{13} (pE and pM), (i) D_{13} (nE and nM), (j) D_{33} (pE and pM).

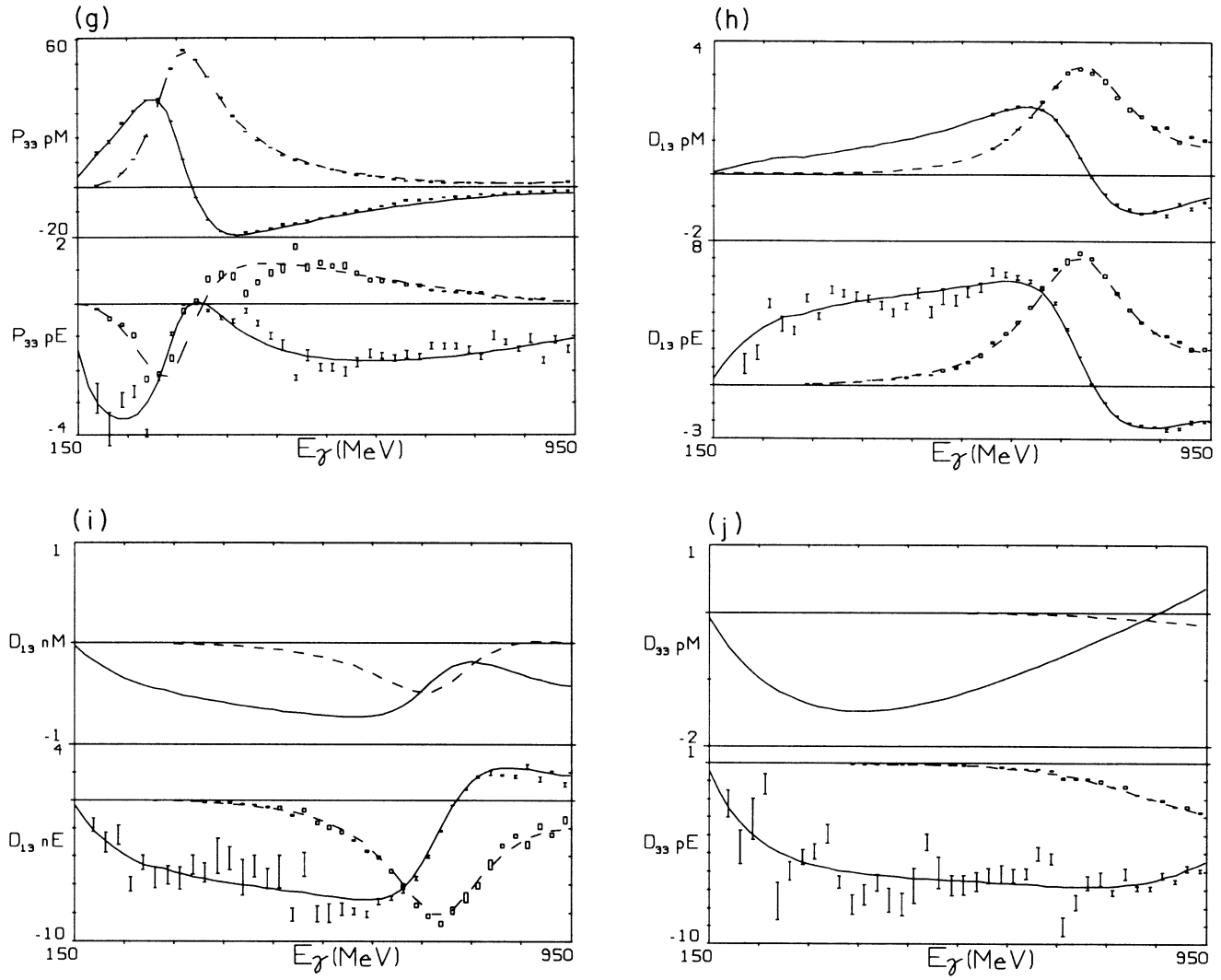

FIG. 2. (*Continued*).

Here P, Σ, and T are, respectively, the asymmetries arising from polarized recoil nucleons, polarized incident photons, and a polarized target. The G and H observables involve both polarized photons and a polarized target. The variables q and k refer, respectively, to the center-of-momentum frame momenta of the pion and the photon.

IV. ENERGY-DEPENDENT PARAMETRIZATION

In order to construct the helicity amplitudes given in Eq. (3.1), we require values for the electric and magnetic multipoles. In the energy-dependent fit we parametrize our multipole amplitudes, denoted by A below, in terms of T_π the T-matrix element for π-N scattering in the appropriate partial wave.

Our energy-dependent parametrization is

$$A = A_I(1+iT_\pi)+A_R T_\pi \ , \tag{4.1}$$

where

$$A_R \equiv \frac{\mu}{q}\left[\frac{k}{q}\right]^l \sum_{n=0}^{N} p_n \left[\frac{E_\pi}{\mu}\right]^n ,$$

$$E_\pi = \frac{s-(\mu+M)^2}{2M} = E_\gamma - \mu\left[1+\frac{\mu}{2M}\right]$$

is the pion laboratory kinetic energy for $\pi+N\rightarrow\gamma+N$, $s\equiv W^2$ is the square of the center-of-mass energy, μ is the pion mass, M is the nucleon mass, E_γ is the photon laboratory energy for $\gamma+N\rightarrow\pi+N$, $A_I \equiv A_B + A_Q$, A_B is a partial wave of the pseudoscalar Born amplitude,[13]

$$A_Q \equiv \sum_{n=0}^{M} \bar{p}_n z Q_{l+n}(z), \quad z\equiv\sqrt{q^2+4\mu^2}/q \ , \tag{4.2}$$

and Q_m is the Legendre function of second kind of order m.

The parameters to be searched in fitting the data are p_n and $\bar{p}_n$.

This parametrization guarantees the following.

(1) When the πN partial wave is elastic the multipole amplitude has the πN phase δ. The phase ϕ of the pion photoproduction amplitude is

$$\tan\phi = \frac{A_R \mathrm{Im}T_\pi + A_I \mathrm{Re}T_\pi}{A_I(1-\mathrm{Im}T_\pi) + A_R \mathrm{Re}T_\pi} = f\frac{\mathrm{Im}T_\pi}{\mathrm{Re}T_\pi}$$
$$= f\tan\delta\ , \tag{4.3}$$

where

$$f \equiv \frac{A_R \mathrm{Im}T_\pi + A_I \mathrm{Re}T_\pi}{A_R \mathrm{Im}T_\pi + A_I \mathrm{Re}T_\pi + A_I \dfrac{\mathrm{Im}T_\pi - |T_\pi|^2}{\mathrm{Re}T_\pi}}\ .$$

Thus, when $f=1$ ($|T_\pi|^2=\mathrm{Im}T_\pi$; i.e., no inelasticity in πN scattering) $\tan\phi=\tan\delta$, or Watson's theorem is satisfied. Thus, our parametrization allows energy-dependent variation from Watson's theorem above the inelastic threshold. (In the first resonance region our parametrization is similar to that of Ref. 14).

(2) The multipole amplitudes have the correct threshold behavior.

(3) The Born term is included as a real partial-wave amplitude for $l > l_{\max}$ and has real and imaginary parts for $l \le l_{\max}$, where $l_{\max}$ is the highest l value for which the multipoles in Eq. (3.1) are searched.

(4) The A_Q term gives the correct analytic structure for two-pion exchange.

One might question the use of a pseudoscalar Born amplitude in our parametrization of the multipoles. However, the difference between a pseudoscalar and pseudovector π-N coupling only affects the low partial waves. We have tried both couplings and find that the phenomenological parameters adjust themselves to give essentially identical results for the multipoles. Thus, this choice has no effect on the results reported in the following sections.

V. OUR SOLUTIONS

Our solution evolved from a procedure of iteration between an energy-dependent solution and "energy-independent" fits to data in 20 MeV bins. We began by initializing our parameters [p_n and $\bar{p}_n$ in Eqs. (4.1) and (4.2)] to fit the 150–450 MeV solution of Smith and de Carvalho.[14,15] The energy range was then incrementally extended as additional parameters were added until an upper energy of 1 GeV was reached. At each step χ^2 minimization was achieved through a variation of these parameters.

The data were then binned in 20 MeV bins. For each bin the moduli and phases of all partial waves were obtained from the energy-dependent solution, as well as energy dependences for moduli and phases. Only the moduli were then varied to fit the data in a bin. (Allowing the phases to also vary did not significantly improve the fits and allowed too many variable parameters for the amount of data in the energy bins.) Which partial-waves' moduli were varied in a bin depended on which partial-wave cross sections in the energy-dependent solution exceeded some specified value. The number of search parameters for a bin thus varied from 14 at 180 MeV to 26 at 980 MeV.

TABLE II. Summary of Energy-Independent fits to data in 20 MeV bins. N_d is the number of data, N_p is the number of searched parameters, and χ^2 (ed) is the χ^2 from our energy-dependent solution.

E_γ	N_d	N_p	χ^2	χ^2 (ed)
180	76	14	74.25	136.68
200	73	15	83.03	159.88
220	170	15	272.57	394.05
240	210	15	383.86	487.42
260	278	16	632.99	787.91
280	321	17	683.71	853.79
300	361	18	821.82	1166.65
320	390	18	928.70	1320.72
340	421	18	853.12	1164.41
360	417	19	838.40	1052.62
380	355	19	629.63	817.94
400	347	19	738.47	862.79
420	324	20	672.89	915.26
440	221	21	444.00	610.02
460	246	21	551.73	658.79
480	168	21	354.35	431.02
500	218	21	526.39	674.21
520	154	21	297.73	433.46
540	209	21	356.04	441.66
560	186	21	292.73	356.55
580	238	21	504.94	641.68
600	257	21	453.84	549.91
620	246	21	437.94	543.03
640	274	21	681.11	835.15
660	328	21	808.40	955.61
680	268	22	626.49	742.66
700	416	22	1170.81	1354.01
720	234	22	421.40	658.30
740	334	23	701.77	985.78
760	331	23	746.72	1035.74
780	218	23	363.07	503.29
800	332	24	729.22	834.46
820	174	24	400.96	465.89
840	282	25	579.69	755.77
860	272	25	568.81	702.76
880	158	25	283.70	497.55
900	268	25	749.21	985.92
920	174	25	377.10	579.36
940	238	25	677.73	874.13
960	228	26	664.62	848.39
980	115	26	296.16	483.38

The energy-independent results were then used to reinitialize the energy-dependent parameters, with care being taken to address any systematic disparities between the energy-dependent and energy-independent fits through the addition of parameters. Another energy-dependent fit was then done, beginning a second cycle. Through this iterative procedure we evolve the energy-dependent fit and the set of energy-independent solutions.

Because of the connection between pion-nucleon elastic scattering and pion photoproduction, we refer to the pion photoproduction states by the notation $L_{2I,2j}$ for πN

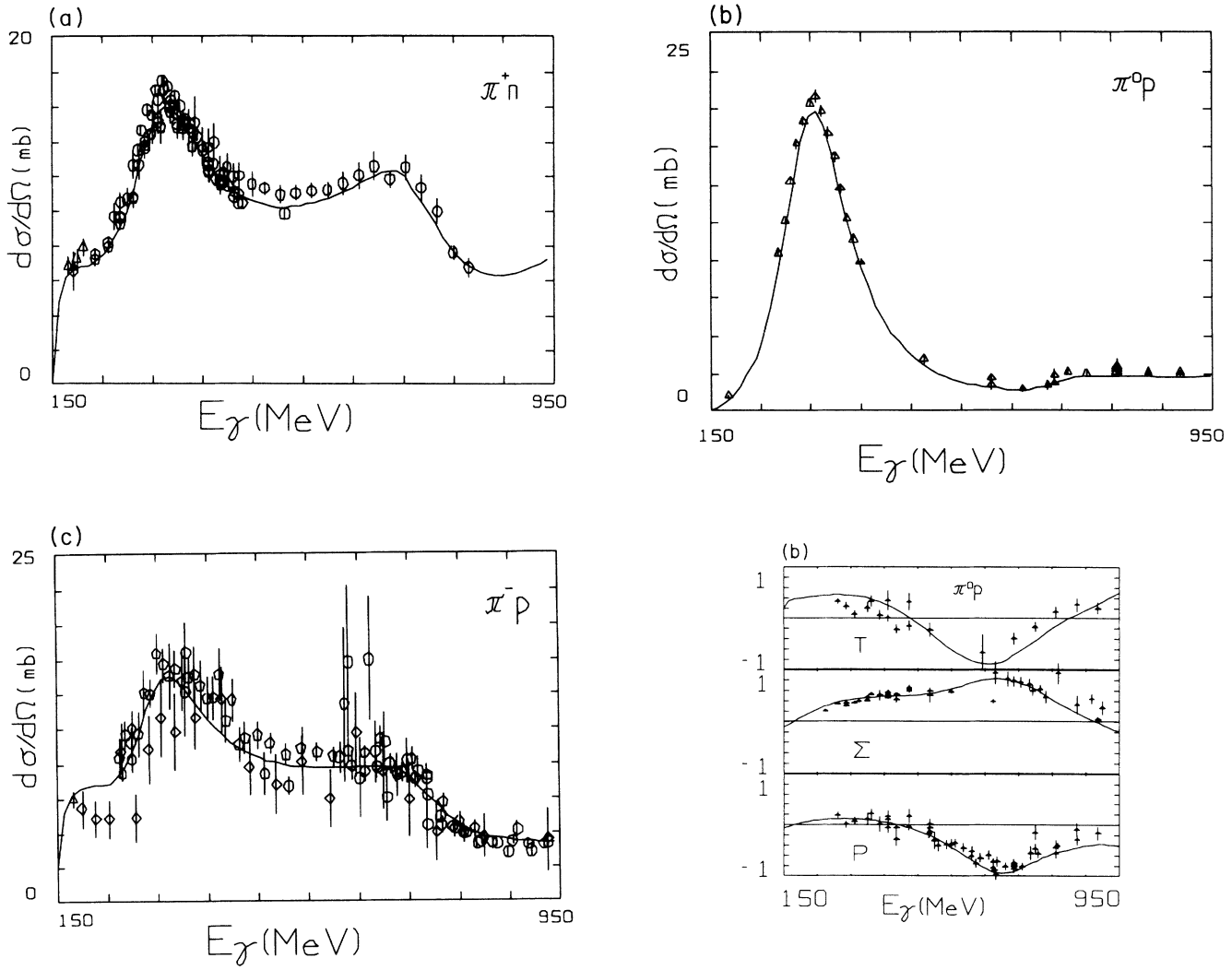

FIG. 3. Observables calculated from our energy dependent solution. Renormalization of the angular data is allowed in the fitting, but the renormalization is not shown in these figures. (a) $\gamma p \rightarrow \pi^+ n$, differential cross section at 45° c.m.; (b) $\gamma p \rightarrow \pi^0 p$, differential cross section, $P(\theta), \Sigma(\theta)$, and $T(\theta)$ at 135° c.m.; (c) $\gamma n \rightarrow \pi^- p$, differential cross section at 45° c.m.

scattering followed by the notation (target, multipole) for pion photoproduction, e.g. $S_{31}pE$. The most important multipole amplitudes for both the energy-dependent and energy-independent solutions are shown in Fig. 2. We do not put errors on the energy-dependent fit as we feel that more realistic errors are those of the energy-independent fits. The S-wave multipoles are shown in Figs. 2(a) and 2(b). Note that the η-production threshold is clearly evident in the S_{11} multipoles. The P-wave multipoles are given in Figs. 2(c) to 2(g). Of these, the $P_{33}pM$ multipole, Fig. 2(g), is very well defined—all recent analyses are in agreement here. The energy-independent solutions for the P_{11} multipoles, Fig. 2(c), in contrast, show considerable scatter about the energy-dependent solution. This is particularly true for $P_{11}nM$ and is true as well for the $P_{31}pM$ multipole displayed in Fig. 2(f). The D_{13} multipoles, Figs. 2(h) and 2(i), show clean resonance behav-

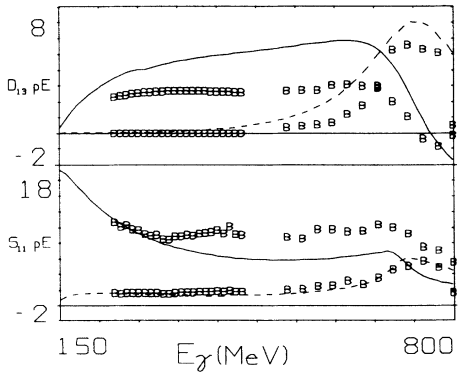

FIG. 4. Comparison of our energy dependent solution with the results of Berends and Donnachie[5] (labeled B) for the $S_{11}pE$ and $D_{13}pE$ multipoles. Notation as in Fig. 2.

ior. It should be noted that the $D_{13}nM$ and $D_{33}pM$ multipoles were not searched in our energy-independent fits as they are quite small. As described above, they were fixed at the values determined from our energy-dependent result during the energy independent analyses. A comparison of the energy-dependent and -independent results is given in Table II.

The data base is quite noisy as evidenced by plotting certain observables and as reflected in the large χ^2 (around 3.5/datum) for the energy-dependent solution. The energy-independent solutions are, on average, about 30% lower in χ^2, but yield amplitudes that scatter statistically about the energy-dependent values, another indication of inconsistent data throughout the base. A representative display of our fits to the various data types is given in Fig. 3. While the overall fit is quite good it is clear, particularly from the polarization observables in Fig. 3(b) and the cross sections in Fig. 3(c), that some data[6] are either inconsistent or require large renormalizations.

A further indication of bad data was obtained through a pruning run in which all data that were more than five standard deviations from the predictions of our solution were located and removed. This resulted in a χ^2 reduction of over 5000 for 133 removed data (about 1.4% of the entire data base). There was no indication from the pruning run that particular data types were being systematically missed or that particular energy ranges were not being fitted by the solution. When the solution was then adjusted to the pruned data set a further reduction of around 500 was accomplished, but the resulting changes in amplitudes were miniscule. The solution, in fact, seems to be quite stable against such cosmetic changes in the data base.

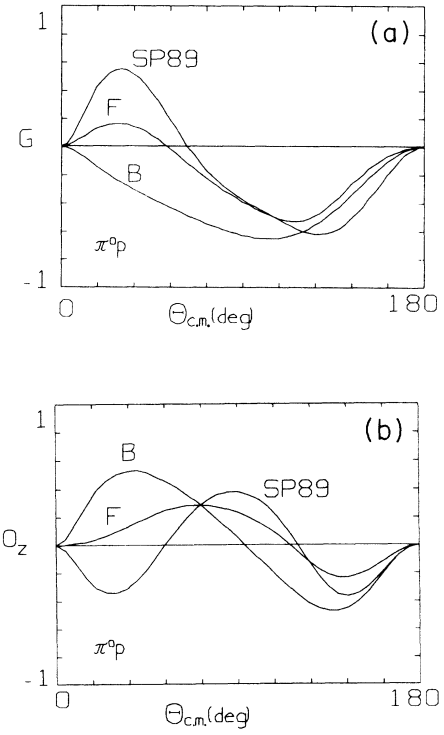

FIG. 5. Comparison of our solution (*SP*), the Berends and Donnachie[5] (*B*) solution, and the Feller *et al.* (Ref. 16) (*F*) solution for $\gamma p \to \pi^0 p$ observables at 750 MeV. (a) $G(\theta)$ observable. (b) $O_z(\theta)$ observable.

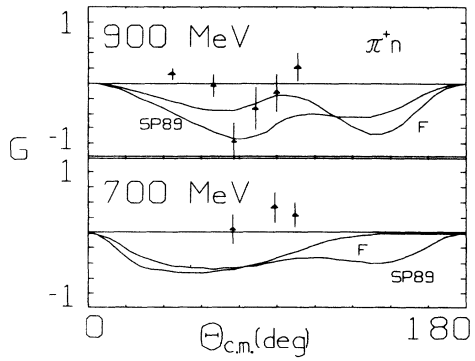

FIG. 6. Comparison of our energy-dependent solution (*SP*) and results of Feller *et al.* (Ref. 16) (*F*) with the observables (Ref. 17) *G* for $\gamma p \to \pi^+ n$ at 700 and 900 MeV.

We have also compared the quality of a 0–500 MeV fit against our solution to 1 GeV. We find that the 0–500 MeV energy-dependent solution gives a χ^2/datum of 2.8 while the fit to 1 GeV results in a χ^2/datum of 3.0 for the same data. Thus, our fit to the low-energy data has not been appreciably degraded in its extension to 1 GeV.

VI. COMPARISONS AND DISCUSSION

Having described our formalism and solutions in some detail, we can now compare our results with the results of previous analyses. We compare mainly with the solutions of Refs. 5 and 16. These authors give their results in terms of multipoles to which we can directly compare. We will also comment on some recent analyses which give their results in terms of radiative decay amplitudes for the underlying resonances.

While we are in reasonable agreement with the P_{33} and P_{11} partial waves of Berends and Donnachie,[5] we find substantial deviations in S_{11} and D_{13}. In Fig. 4, we compare our results for the $S_{11}pE$ and $D_{13}pE$ multipoles with those given in Ref. 5. From these multipoles, Berends and Donnachie found for the radiative decay amplitudes $A^p_{1/2}$ of the $S_{11}(1535)$ and $A^p_{3/2}$ of the $D_{13}(1520)$, about half the current Particle Data Group average values. We generally find the older analysis of Feller *et al.*[16] to be in better agreement with our results. Figure 5 shows the observables[12] *G* and O_z for the $\gamma p \to p\pi^0$ reaction at 750 MeV. We found these to be quite sensitive to differences between our results and the results of Refs. 5 and 16. As no data exists in this region, measurements would be desirable. A measurement of these observables at 35° with an accuracy of ± 0.1 might help to differentiate between these solutions.

Some measurements of the double polarization observables *G* and *H* now exist. However, as can be seen in Fig. 1, they are quite sparse and only exist, in our energy range, for the $\gamma p \to n\pi^+$ reaction. While our fit to the

existing H data is reasonable, we find that at several energies the fit to G is very poor. In Fig. 6, we show a comparison between the present solution, the results of Feller *et al.*,[16] and the data of Ref. 17. At 700 and 900 MeV the fit of Ref. 16 qualitatively agrees with our solution. Particularly at 700 MeV, however, there are serious conflicts with the data. We should point out that the experimental data[17] were originally compared[17] with the results of Barbour, Crawford, and Parsons[1] and that the conflict evident in Fig. 6 existed for this analysis as well. A remeasurement of this data would clearly be useful.

Recently, precise left-right asymmetry (A_N) data from the reaction $\pi^- p \to n\gamma$ have become available.[9] The observable A_N is related by time-reversal invariance to the polarization (P) measured in $\gamma n \to \pi^- p$. Use of this inverse reaction has the advantage that a deuterium target is not required. In comparing their[9] measured values to the predictions of Arai and Fujii,[3] Noelle,[18] and the present analysis, it was found[9] that both the present analysis and the analysis of Noelle[18] were in good agreement. The agreement with Arai and Fujii[3] was found to be poor, particularly near 600 MeV/c. This is interesting as the analysis of Noelle[18] is more than twelve years old and was completed prior to the work of Arai and Fujii.[3] As is noted in Ref. 9, this also reflects on the radiative decay amplitude for the $P_{11}(1440)$. The amplitude $A^n_{1/2}$ deduced for this resonance from the analysis of Noelle[18] and from the present analysis[19] is found to agree with the recent Glasgow analysis.[2] The Arai and Fujii[3] result ($23\pm9\times10^{-3}$ GeV$^{-1/2}$) is only half as large.

In summary, we have found that our results deviate considerably from those of Refs. 3 and 5. From those comparisons we have been able to make, we seem to be in better agreement with the analyses of Noelle[18] and the recent Glasgow analyses.[1,2] Future experimental investigations of double polarization observables, G in particular, would be desirable in order to select between the existing analyses and to confirm those measurements which currently exist. In addition, a continuation of the program to measure the reaction $\pi^- p \to n\gamma$ is important as a check on measurements made with deuteron targets. It is conceivable that the combination of deuteron and $\pi^- p \to n\gamma$ data will also reveal additional information on the deuteron itself.

APPENDIX A: CONNECTION BETWEEN MULTIPOLE AMPLITUDES AND HELICITY AMPLITUDES

In this paper we have used the electric and magnetic multipole amplitudes as basic elements in our analyses. Another approach is to use the helicity partial-wave amplitudes $A_{l\pm}$ and $B_{l\pm}$, which are related to the multipoles through the relations[11]

$$A_{l+}=\tfrac{1}{2}[(l+2)E_{l+}+lM_{l+}] ,$$

$$B_{l+}=E_{l+}-M_{l+} ,$$

$$A_{(l+1)-}=\tfrac{1}{2}[(l+2)M_{(l+1)-}-lE_{(l+1)-}] ,$$

and

$$B_{(l+1)-}=E_{(l+1)-}+M_{(l+1)-} .$$

Note that in the notation of Bransden and Moorhouse[20] B_{l+} and $B_{(l+1)-}$ have an extra factor of $2/\sqrt{l(l+2)}$. Moorhouse, Oberlack, and Rosenfeld[10] have given their solutions in terms of isoscalar (A^s) and isovector (A^{V_1}, A^{V_3}) amplitudes. These are related to helicity amplitudes with our isospin convention via:

$$A^{3/2}=\sqrt{\tfrac{3}{2}}A^{V_3} ,$$

$${}_pA^{1/2}=\sqrt{\tfrac{1}{3}}(A^{V_1}-A^s) ,$$

and

$${}_nA^{1/2}=\sqrt{\tfrac{1}{3}}(A^{V_1}+A^s) .$$

Various factors of m_π, $\hbar c$, and $\sqrt{qk}$ are required to match the units of previous solutions. For example, the multipoles of Berends and Donnachie[5] are related to ours (reported in millifermi units) by a factor of $1000\,\hbar c/\mu c^2$. See also Appendix B of Moorhouse, Oberlack, and Rosenfeld.[10]

APPENDIX B: MOTIVATION FOR THE ENERGY-DEPENDENT PARAMETRIZATION

Our parametrization, Eq. (4.1), is motivated by the way in which the πN interaction is parametrized by our group. A coupled-channel K-matrix approach is used to couple the πN elastic channel to an inelastic channel, which we refer to below as a $\pi\Delta$ channel although the ηN channel also occurs for the S_{11} state. The 2×2 hadronic K and T matrices are written as

$$K_h=\begin{bmatrix} K_{\pi\pi} & K_{\pi\Delta} \\ K_{\pi\Delta} & K_{\Delta\Delta} \end{bmatrix}$$

and

$$T=\begin{bmatrix} T_{\pi\pi} & T_{\pi\Delta} \\ T_{\pi\Delta} & T_{\Delta\Delta} \end{bmatrix}=K_h(1-iK_h)^{-1} .$$

It can be shown that $T_{\pi\pi}$ can be expressed in terms of a K function, $\bar{K}$, as

$$T_{\pi\pi}=\frac{\bar{K}}{1-i\bar{K}}, \tag{B1}$$

where

$$\bar{K}=K_{\pi\pi}+\frac{iK^2_{\pi\Delta}}{1-iK_{\Delta\Delta}}=\frac{T_{\pi\pi}}{1+iT_{\pi\pi}}$$

and that

$$T_{\pi\Delta}=\frac{K_{\pi\Delta}}{1-iK_{\Delta\Delta}}(1+iT_{\pi\pi}) .$$

If we expand to a 3×3 K matrix of the form

$$K=\begin{bmatrix} K_{\gamma\gamma} & K_{\gamma\pi} & K_{\gamma\Delta} \\ K_{\gamma\pi} & K_{\pi\pi} & K_{\pi\Delta} \\ K_{\gamma\Delta} & K_{\pi\Delta} & K_{\Delta\Delta} \end{bmatrix}$$

and use the relationship Eq. (3.4) of Noelle,[18] then

$$T_{\gamma\pi}(1-iK_{\gamma\gamma})=(1+iT_{\pi\pi})K_{\gamma\pi}+iK_{\gamma\Delta}T_{\pi\Delta}$$
$$=(1+iT_{\pi\pi})\left[K_{\gamma\pi}+i\frac{K_{\gamma\Delta}}{K_{\pi\Delta}}\frac{K_{\pi\Delta}^2}{1-iK_{\Delta\Delta}}\right]. \quad \text{(B2)}$$

Inserting Eq. (B1) yields

$$(1-iK_{\gamma\gamma})T_{\gamma\pi}=(1+iT_{\pi\pi})\left[K_{\gamma\pi}-\frac{K_{\gamma\Delta}K_{\pi\pi}}{K_{\pi\Delta}}\right]+\frac{K_{\gamma\Delta}}{K_{\pi\Delta}}T_{\pi\pi}$$
$$\equiv A_I(1+iT_\pi)+A_R T_\pi\ . \quad \text{(B3)}$$

For $K_{\gamma\gamma}=0$, this is the expression, Eq. (4.1), we use for our parametrization. Note that both $K_{\gamma\Delta}$ and $K_{\pi\Delta}$ have a branch point at the inelastic Δ threshold and become complex for lower energies, but their ratio remains real below the inelastic branch point because of the cancellation of the momentum transfer to the Δ raised to the same power. Thus, the coefficients A_I and A_R are real.

[1] I. M. Barbour, R. L. Crawford, and N. H. Parsons, Nucl. Phys. **B141**, 253 (1978).

[2] R. L. Crawford and W. T. Morton, Nucl. Phys. **B211**, 1 (1983).

[3] I. Arai and H. Fujii, Nucl. Phys. **B194**, 251 (1982).

[4] V. F. Grushin *et al.*, Yad. Fiz. **38**, 1448 (1983) [Sov. J. Nucl. Phys. **38**, 881 (1983)].

[5] F. A. Berends and A. Donnachie, Nucl. Phys. **B84**, 342 (1975); **B136**, 317 (1978).

[6] More detailed information concerning the data base and the multipole amplitudes is available from the authors upon request or interactively through the Scattering Analysis Interactive Dial-in (SAID) program.

[7] K. Ukai and T. Nakamura, Institute for Nuclear Study, University of Tokyo, Japan Report No. INS-TEC-22 (1985). We have obtained an updated tape of this compilation from INS, University of Tokyo.

[8] D. Menze, W. Pfeil, and R. Wilcke, Physikalisches Institut der Universität Bonn, Germany, Physik Daten 7-1 (1977).

[9] G. J. Kim *et al.*, UCLA Report UCLA-10-P25-179 (unpublished); B. M. K. Nefkens, private communication.

[10] R. G. Moorhouse, H. Oberlack, and A. H. Rosenfeld, Phys. Rev. D **9**, 1 (1974).

[11] R. L. Walker, Phys. Rev. **182**, 1729 (1969).

[12] I. S. Barker, A. Donnachie, and J. K. Storrow, Nucl. Phys. **B95**, 347 (1975).

[13] F. A. Berends, A. Donnachie, and D. L. Weaver, Nucl. Phys. **B4**, 1 (1967).

[14] A. W. Smith and N. Zagury, Phys. Rev. D **20**, 2719 (1979); **21**, 2514 (1980).

[15] A. W. Smith and F. A. B. R. De Carvalho, Nuovo Cim. **88A**, 100 (1985).

[16] P. Feller, M. Fukushima, N. Horikawa, R. Kajikawa, K. Mori, T. Nakanishi, T. Ohshima, C. O. Pak, M. Saito, S. Suzuki, Y. Tarui, T. Yamaki, T. Matsuda, K. Mizushima, and N. Tokuda, Nucl. Phys. **B104**, 219 (1976).

[17] P. J. Bussey *et al.*, Nucl. Phys. **B169**, 403 (1980).

[18] P. Noelle, Prog. Theor. Phys. **60**, 778 (1978).

[19] R. A. Arndt, R. L. Workman, Z. Li, and L. D. Roper, Phys. Rev. C **42**, 1864 (1990), the following article.

[20] B. H. Bransden and R. G. Moorhouse, *The Pion-Nucleon System* (Princeton University Press, Princeton, NJ, 1973).